Research Article | Vol. 9, No. 5 | 1 May 2018 | BIOMEDICAL OPTICS EXPRESS 2304
Biomedical Optics EXPRESS

Fiber-based tunable repetition rate source for deep tissue two-photon fluorescence microscopy

KRITI CHARAN,[1] BO LI,[1] MENGRAN WANG,[1] CHARLES P. LIN,[2] AND CHRIS XU[1*]

[1]*School of Applied Physics and Engineering, Cornell University, Ithaca, NY 14850, USA*
[2]*Wellman Center for Photomedicine and Center for Systems Biology, Massachusetts General Hospital, Harvard Medical School, Boston, MA 02115, USA*
**cx10@cornell.edu*

Abstract: Deep tissue multiphoton imaging requires high peak power to enhance signal and low average power to prevent thermal damage. Both goals can be advantageously achieved through laser repetition rate tuning instead of simply adjusting the average power. We show that the ideal repetition rate for deep two-photon imaging in the mouse brain is between 1 and 10 MHz, and we present a fiber-based source with an arbitrarily tunable repetition rate within this range. The performance of the new source is compared to a mode-locked Ti:Sapphire (Ti:S) laser for *in vivo* imaging of mouse brain vasculature. At 2.5 MHz, the fiber source requires 5.1 times less average power to obtain the same signal as a standard Ti:S laser operating at 80 MHz.

© 2018 Optical Society of America under the terms of the OSA Open Access Publishing Agreement

OCIS codes: (180.4315) Nonlinear microscopy; (320.7090) Ultrafast lasers.

References and links

1. D. Kobat, M. E. Durst, N. Nishimura, A. W. Wong, C. B. Schaffer, and C. Xu, "Deep tissue multiphoton microscopy using longer wavelength excitation," Opt. Express **17**(16), 13354–13364 (2009).
2. F. Helmchen and W. Denk, "Deep tissue two-photon microscopy," Nat. Methods **2**(12), 932–940 (2005).
3. P. Theer, M. T. Hasan, and W. Denk, "Two-photon imaging to a depth of 1000 µm in living brains by use of a $Ti:Al_2O_3$ regenerative amplifier," Opt. Lett. **28**(12), 1022–1024 (2003).
4. D. R. Miller, A. M. Hassan, J. W. Jarrett, F. A. Medina, E. P. Perillo, K. Hagan, S. M. Shams Kazmi, T. A. Clark, C. T. Sullender, T. A. Jones, B. V. Zemelman, and A. K. Dunn, "*In vivo* multiphoton imaging of a diverse array of fluorophores to investigate deep neurovascular structure," Biomed. Opt. Express **8**(7), 3470–3481 (2017).
5. D. A. Dombeck, A. N. Khabbaz, F. Collman, T. L. Adelman, and D. W. Tank, "Imaging Large-Scale Neural Activity with Cellular Resolution in Awake, Mobile Mice," Neuron **56**(1), 43–57 (2007).
6. W. Mittmann, D. J. Wallace, U. Czubayko, J. T. Herb, A. T. Schaefer, L. L. Looger, W. Denk, and J. N. D. Kerr, "Two-photon calcium imaging of evoked activity from L5 somatosensory neurons *in vivo*," Nat. Neurosci. **14**(8), 1089–1093 (2011).
7. C. Tischbirek, A. Birkner, H. Jia, B. Sakmann, and A. Konnerth, "Deep two-photon brain imaging with a red-shifted fluorometric Ca^{2+} indicator," Proc. Natl. Acad. Sci. U.S.A. **112**(36), 11377–11382 (2015).
8. V. Gautam, J. Drury, J. M. C. Choy, C. Stricker, H.-A. Bachor, and V. R. Daria, "Improved two-photon imaging of living neurons in brain tissue through temporal gating," Biomed. Opt. Express **6**(10), 4027–4036 (2015).
9. R. Prevedel, A. J. Verhoef, A. J. Pernía-Andrade, S. Weisenburger, B. S. Huang, T. Nöbauer, A. Fernández, J. E. Delcour, P. Golshani, A. Baltuska, and A. Vaziri, "Fast volumetric calcium imaging across multiple cortical layers using sculpted light," Nat. Methods **13**(12), 1021–1028 (2016).
10. C. Xu, W. Zipfel, J. B. Shear, R. M. Williams, and W. W. Webb, "Multiphoton fluorescence excitation: new spectral windows for biological nonlinear microscopy," Proc. Natl. Acad. Sci. U.S.A. **93**(20), 10763–10768 (1996).
11. K. Podgorski and G. Ranganathan, "Brain heating induced by near-infrared lasers during multiphoton microscopy," J. Neurophysiol. **116**(3), 1012–1023 (2016).
12. N. G. Horton, K. Wang, D. Kobat, C. G. Clark, F. W. Wise, C. B. Schaffer, and C. Xu, "*In vivo* three-photon microscopy of subcortical structures within an intact mouse brain," Nat. Photonics **7**(3), 205–209 (2013).
13. C. Xu and W. W. Webb, "Measurement of two-photon excitation cross sections of molecular fluorophores with data from 690 to 1050 nm," J. Opt. Soc. Am. B **13**(3), 481–491 (1996).
14. Spectra-Physics, "Femtosource XL."

#320925 https://doi.org/10.1364/BOE.9.002304
Journal © 2018 Received 30 Jan 2018; revised 16 Apr 2018; accepted 17 Apr 2018; published 23 Apr 2018

Biomedical Optics EXPRESS

15. Coherent, "Mira-900 with pulse switch accessory."
16. R. J. Jones and J. Ye, "Femtosecond pulse amplification by coherent addition in a passive optical cavity," Opt. Lett. **27**(20), 1848–1850 (2002).
17. J. P. Gordon, F. M. Mitschke, and L. F. Mollenauer, "Discovery of the soliton self-frequency shift," Opt. Lett. **11**(10), 662–664 (1986).
18. P. Beaud, W. Hodel, B. Zysset, and H. P. Weber, "Ultrashort pulse propagation, pulse breakup, and fundamental soliton formation in a single-mode optical fiber," IEEE J. Quantum Electron. **23**(11), 1938–1946 (1987).
19. J. H. Lee, J. van Howe, X. Liu, and C. Xu, "Soliton self-frequency shift: experimental demonstrations and applications," IEEE J. Sel. Top. Quantum Electron. **14**(3), 713–723 (2008).
20. H. Tu and S. A. Boppart, "Versatile photonic crystal fiber-enabled source for multi-modality biophotonic imaging beyond conventional multiphoton microscopy," Proc. SPIE **7569**, 75692D (2010).
21. K. Wang, N. G. Horton, K. Charan, and C. Xu, "Advanced fiber soliton sources for nonlinear deep tissue imaging in biophotonics," IEEE J. Sel. Top. Quantum Electron. **20**, 6800311 (2014).
22. C. Xu, J. Guild, W. Webb, and W. Denk, "Determination of absolute two-photon excitation cross sections by in situ second-order autocorrelation," Opt. Lett. **20**(23), 2372 (1995).
23. D. Sinefeld, H. P. Paudel, D. G. Ouzounov, T. G. Bifano, and C. Xu, "Adaptive optics in multiphoton microscopy: comparison of two, three and four photon fluorescence," Opt. Express **23**(24), 31472–31483 (2015).
24. G. H. Patterson and D. W. Piston, "Photobleaching in two-photon excitation microscopy," Biophys. J. **78**(4), 2159–2162 (2000).
25. A. Hopt and E. Neher, "Highly nonlinear photodamage in two-photon fluorescence microscopy," Biophys. J. **80**(4), 2029–2036 (2001).
26. N. Ji, J. C. Magee, and E. Betzig, "High-speed, low-photodamage nonlinear imaging using passive pulse splitters," Nat. Methods **5**(2), 197–202 (2008).
27. F. F. Voigt, F. Emaury, P. Bethge, D. Waldburger, S. M. Link, S. Carta, A. van der Bourg, F. Helmchen, and U. Keller, "Multiphoton *in vivo* imaging with a femtosecond semiconductor disk laser," Biomed. Opt. Express **8**(7), 3213–3231 (2017).
28. P. Xi, Y. Andegeko, L. R. Weisel, V. V. Lozovoy, and M. Dantus, "Greater signal, increased depth, and less photobleaching in two-photon microscopy with 10 fs pulses," Opt. Commun. **281**(7), 1841–1849 (2008).
29. J. J. Field, R. Carriles, K. E. Sheetz, E. V. Chandler, E. E. Hoover, S. E. Tillo, T. E. Hughes, A. W. Sylvester, D. Kleinfeld, and J. A. Squier, "Optimizing the fluorescent yield in two-photon laser scanning microscopy with dispersion compensation," Opt. Express **18**(13), 13661–13672 (2010).
30. D. J. L. Graham, S. F. Tseng, J. T. Hsieh, D. J. Chen, and G. Alexandrakis, "Dependence of Two-Photon eGFP Bleaching on Femtosecond Pulse Spectral Amplitude and Phase," J. Fluoresc. **25**(6), 1775–1785 (2015).
31. G. Donnert, C. Eggeling, and S. W. Hell, "Major signal increase in fluorescence microscopy through dark-state relaxation," Nat. Methods **4**(1), 81–86 (2007).
32. R. Le Harzic, I. Riemann, K. König, C. Wüllner, and C. Donitzky, "Influence of femtosecond laser pulse irradiation on the viability of cells at 1035, 517, and 345 nm," J. Appl. Phys. **102**, 114701 (2007).
33. J. M. Dela Cruz, J. D. McMullen, R. M. Williams, and W. R. Zipfel, "Feasibility of using multiphoton excited tissue autofluorescence for *in vivo* human histopathology," Biomed. Opt. Express **1**(5), 1320–1330 (2010).
34. G. Olivié, D. Giguère, F. Vidal, T. Ozaki, J.-C. Kieffer, O. Nada, and I. Brunette, "Wavelength dependence of femtosecond laser ablation threshold of corneal stroma," Opt. Express **16**(6), 4121–4129 (2008).
35. N. Linz, S. Freidank, X.-X. Liang, and A. Vogel, "Wavelength dependence of femtosecond laser-induced breakdown in water and implications for laser surgery," Phys. Rev. B **94**(2), 024113 (2016).

1. Introduction

Two-photon microscopy has become an invaluable tool in biological imaging. Its many advantages include diffraction-limited resolution with optical sectioning, fast imaging speeds, and deep penetration through scattering tissues. It has been used to image to depths of ~1mm in the mouse brain [1–4]. With the development of Calcium sensitive probes, it is now possible to observe neuronal activity in real time from deep layers of mouse cortex [5–7].

Penetration of excitation light in biological tissues is limited by attenuation due to scattering and absorption. As imaging depth increases, power at the surface must be increased exponentially to compensate for the decreasing number of ballistic photons reaching the focal volume. Typically, this is done by increasing the average power at the surface of the brain. However, using too much average power raises the sample's temperature, potentially causing thermal damage in the superficial layers.

A better approach to achieve maximum fluorescence excitation without significant heating is to reduce the laser repetition rate and increase the pulse energy, while keeping the average power at the surface of the brain fixed [8,9]. Temporal redistribution of the incident photons in this manner enhances nonlinear effects (multiphoton excitation) without changing the linear effects (sample heating). Because the ideal repetition rate depends on the imaging depth

Biomedical Optics EXPRESS

(as shown in the next section), there is an urgent need to develop a tunable repetition rate source to ensure optimum imaging conditions can be achieved across a range of imaging depths.

2. Ideal repetition rate for two-photon deep tissue imaging

The upper limit for the laser repetition rate is typically determined by the lifetime of the dye, τ_f. In the regime where $f\tau_f > 1$, excitation pulses arrive before most of the excited fluorophores have relaxed. Thus the fluorescence signal generated may not have the expected linear dependence on the repetition rate when the probability of excitation per pulse is relatively high [10]. Most fluorescent dyes have lifetimes in the range of 1-10 nanoseconds, indicating that the typical repetition rate should be below 100 MHz.

At the lower end, one must balance linear thermal damage due to volume heating, fluorescence saturation and nonlinear damage at the focus. At near infrared wavelengths, it was determined that ~100 mW average power is safe for long term, continuous imaging in the mouse brain [11]. For two-photon microscopy using femtosecond pulses, the condition for fluorescence saturation sets the limit of pulse energy (typically < 1 nJ at the focus of an objective lens with an NA of ~1.0).

The optimum repetition rate (f_o) of the excitation source for two-photon imaging is determined by the need to obtain maximum fluorescence signal while staying below the power limit for significant sample heating and the pulse-energy limit for fluorophore saturation. f_o can be determined by the following parameters: imaging depth (z), tissue attenuation length (l_a, which depends on the scattering and absorption lengths [12]), average power limit for thermal damage $<P_{surface}>$, and pulse energy limit for fluorescence saturation (E_{sat}). The relation between the parameters is given by the equation:

$$f_0 \approx \frac{\langle P_{surface} \rangle}{E_{focus}} \exp\left(\frac{-z}{l_a}\right) \tag{1}$$

The pulse energy at the focus, E_{focus}, should be substantially below E_{sat}, which can be calculated following ref. 13:

$$E_{sat} = \frac{\lambda^2}{\pi NA^2}\sqrt{\frac{\tau}{g_p^{(2)}\sigma_2}} \tag{2}$$

E_{sat} is determined by the excitation wavelength (λ), the objective numerical aperture (NA) assuming diffraction-limited focus, pulse width (τ), the fluorophore two-photon cross-section (σ_2), and the temporal coherence factor $g_p^{(2)}$ ($g_p^{(2)} = 0.59$ for a $sech^2$ and 0.66 for a Gaussian pulse).

Table 1. Saturation pulse energy E_{sat} and the optimum repetition rate, f_0, for imaging at depths of 4 and 5 attenuation lengths (l_a) for some common green and yellow fluorescent dyes.*

Dye	Cross-section (GM)	E_{sat} (nJ)	f_0 (MHz)	
			$l_a = 4$	$l_a = 5$
wtGFP	3	1.34	4.6	1.68
Fluorescein	22	0.49	12.5	4.58
Ca Green	56	0.31	19.7	7.25
YFP	186	0.17	35.9	13.2

* Assumptions: Diffraction-limited focus with NA = 1.0, λ = 940 nm, $P_{surface}$ = 100 mW, Gaussian temporal pulse intensity profile with FWHM τ = 100 fs, and $E_{focus} = 0.3*E_{sat}$.

Equation (1) clearly shows that the optimum repetition rate for deep tissue two-photon microscopy decreases exponentially with the imaging depth. $E_{focus}/E_{sat} < 0.3$ results in less

Biomedical Optics EXPRESS

than 5% deviation from true quadratic dependence on the excitation power in a diffraction-limited focused beam. E_{sat} for some common dyes [13] and corresponding f for imaging at depths of 4 and 5 attenuation lengths are given in the Table 1. The values in Table 1 show that the optimum repetition rate is significantly lower than that typically provided by a femtosecond mode-locked Ti:S laser (e.g., 80 MHz).

3. Pulse energy requirements for deep tissue imaging

We now estimate the pulse energy required from the excitation source for deep tissue two-photon imaging, using fluorescein as an example. In order to deliver 0.15 nJ to the focus (i.e., $0.3*E_{sat}$ for fluorescein) at a depth of five attenuation lengths one must start with ~50-110 nJ before the microscope (assuming 20-45% microscope transmission). Such high pulse energies are marginally achievable with commercially available Ti:S lasers at the peak gain wavelength of ~800 nm, but their performance rapidly degrades at longer wavelengths, and the required pulse energy is hard to realize for wavelengths > 900 nm. Several systems can generate higher pulse energies, but few can provide the right combination of wavelength tuning, repetition rate, and pulse energy for optimum deep tissue two-photon imaging. Optical parametric amplifier (OPA) pumped by an amplifier system can provide wavelength tunable pulses at > 1μJ, however, OPAs are expensive, and their highest repetition rate is typically limited to 1 to 2 MHz, which limits the imaging speed for studying dynamic biological functions such as neuronal activity and blood flow [3,4]. Extended cavity lasers can provide >100 nJ pulse energies and 1-10 MHz repetition rates, but the wavelength tuning in these systems is limited to ~10 nm around 800 nm [14]. Cavity dumped lasers are also commercially available, however, the pulse energy available drops to < 50 nJ as one increases the repetition rate into the few MHz range [15]. Although coherent addition in an external passive cavity has been demonstrated with impressive results, the system has not seen widespread deployment [16]. In summary, wavelength-tunable sources at > 900 nm (the wavelength window of interest for a large number of brain imaging applications) that can provide more than 50 nJ pulse energy with repetition rate tunable within the range of 1 to 10 MHz do not exist currently, but are needed for optimum deep tissue two-photon imaging.

4. Fiber-based tunable repetition rate source for deep tissue two-photon fluorescence microscopy

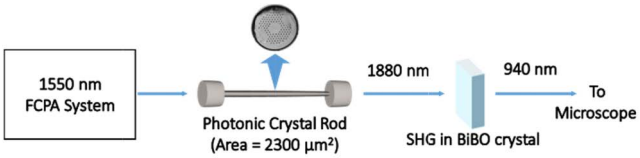

Fig. 1. Tunable repetition rate source for two-photon imaging.

We demonstrate a fiber-based laser system that can provide both tunable repetition rate between 1 and 10 MHz, and high pulse energies for wavelengths > 900 nm (Fig. 1). The source consists of a 1550 nm fiber chirped pulse amplification (FCPA) system that pumps a photonic crystal rod (PC Rod). Erbium-doped fiber amplifier based FCPA system is a mature and robust technology. Commercial systems providing > 1 μJ pulse energies, ~500 fs pulses are routinely available. However, the average power from these systems tends to be limited. Our home-built system provides high average power (up to 8 W), allowing it to support the higher repetition rates for fast imaging. The second-order interferometric autocorrelation measurement shows that the FWHM pulse duration of the FCPA system is ~500 fs at 1550 nm.

Repetition rate tuning was achieved using a fiber-integrated Lithium Niobate ($LiNBO_3$) intensity modulator driven by a pulse pattern generator (MU181020A, Anritsu) synchronized

Biomedical Optics EXPRESS

to the seed laser. Placing the intensity modulator before the final amplification stages ensures that no optical power from the power amplifiers is wasted when adjusting the repetition rate.

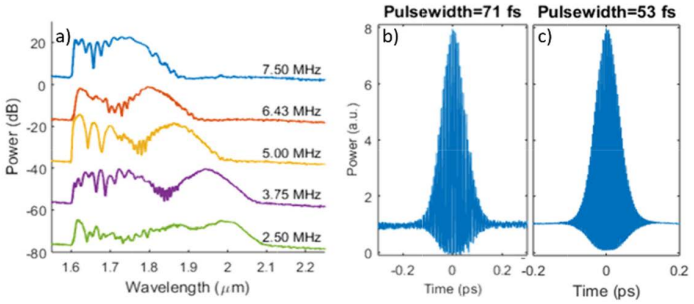

Fig. 2. a) SSFS spectra after the PC Rod at various repetition rates when pumped at 7W of average power at 1550 nm. A 1600-nm long pass filter was used to remove the residual pump light. Spectra are offset vertically for clarity. Second order interferometric autocorrelations for the 1880 nm soliton (b, deconvolution factor = 1.54) and the 940 nm frequency-doubled pulse (c, deconvolution factor = 1.4).

Soliton self-frequency shift (SSFS) in optical fibers produces wavelength-tunable $sech^2$ pulses [17–20]. The soliton energy is proportional to the effective area (A_{eff}) of the mode within the fiber. For our demonstration we used a photonic crystal (PC) rod with a core size of 70 μm (DC-200–70-PMYb-ROD, NKT Photonics). SSFS in this rod has been demonstrated and characterized in [21]. The A_{eff} of the PC Rod is 2300 μm^2 and the rod length is 37 cm. Spectral filters can be used to cleanly separate the solitons from the residual 1550 nm light for soliton center wavelengths longer than 1650 nm. We were able to generate solitons between 1660 nm (55 nJ) and 2000 nm (134 nJ). The maximum repetition rates achievable (limited by the maximum average power of the FCPA) for different soliton center wavelengths, along with the spectra, are shown in Fig. 2(a). The intensity stability of the soliton is measured using two-photon excited photocurrent in a Si-diode. We found that the root-mean-squared (RMS) fluctuation of the soliton pulse is less than 1% when measured for 10 minutes at a sampling rate of 100 kHz. The wavelength stability is measured using a spectrometer, which shows that the RMS fluctuation of the center wavelength of the soliton is less than 1 nm when measured for 20 minutes at 2 wavelength scans/s. The beam pointing stability is confirmed by using a camera to record the center position of the beam.

To double the frequency of the soliton, we used a 1 mm thick BiB_3O_6 crystal ($\theta = 9.8°$, $\varphi = 0°$, Castech). Due to the high pulse energy of the soliton, the conversion efficiency was > 50%. At 940 nm, the maximum pulse energy obtained was 72 nJ, and the pulse duration was 53 fs. The second-order autocorrelation of the soliton and the frequency-doubled pulse from the soliton source are also shown in Fig. 2. As the analysis in Section 3 has shown, the characteristics of such a source are ideally matched for deep tissue two-photon imaging of green and yellow fluorophores such as GCaMPs, GFPs and YFPs.

5. Performance comparison

The output soliton spectrum is determined by the characteristics of the input pulse (pulse energy, pulse shape, and wavelength) and the PC rod (length, A_{eff}, and dispersion), and is independent of the pulse repetition rate. Therefore, the repetition rate can be tuned up to the maximum repetition rate (shown in Fig. 2(a)) without changing the output spectra. We tested the dependence of the fluorescence signal on the laser repetition rate at a constant excitation power, using fluorescein dye solution as the sample (Fig. 3). The small deviations from the perfect linear dependence on *1/f* are probably caused by the difference in the input pulse characteristics due to variations in the nonlinear phase accumulation in the EDFA at different repetition rates and in the coupling of the pulses into the PC rod. To demonstrate the

Biomedical Optics EXPRESS

performance of this tunable repetition rate source, we compared its imaging performance to a commercially available Ti:S oscillator (Maitai, Deep See, SpectraPhysics). The soliton repetition rate was set to 2.5 MHz. The center wavelength for both lasers was set to 940 nm. Both beams were sent into a commercial multiphoton microscope (FV-1000, Olympus). A flip mirror was used to switch between the soliton source and the Ti:S laser.

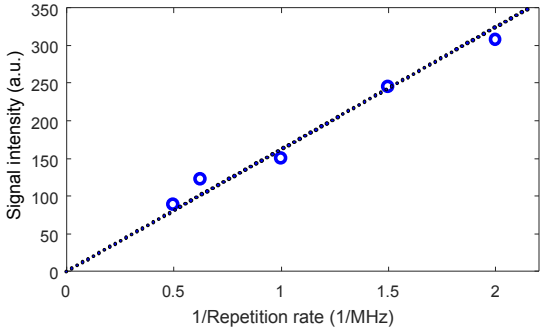

Fig. 3. Fluorescence signal intensity as a function of the inverse of the source repetition rate at the constant average power of 0.08 mW on the sample. The solid circles are the measured data, and the dashed line is a linear fit to the data.

Dispersion from the microscope optics and the objective (XLPN25XWMP2, 25X, 1.05 NA Water Immersion, Olympus) was pre-compensated using a prism pair (80 cm separation) for the soliton source, and the built-in Deep See dispersion compensator in the Ti:S laser. A second-order interferometric autocorrelation measurement performed after the objective showed that the final pulse widths were 76 fs for the soliton source, and 123 fs for the Ti:S (Fig. 4). Wings in the autocorrelation of the soliton source indicate some uncompensated higher order dispersion from the microscope optics. To quantify its effect on two-photon signal generation, we calculated $g_p^{(2)}$ from the second order autocorrelations as described in [22]. Measured $g_p^{(2)}$ for the Ti:S laser pulse and the soliton pulse before the microscope are within ~5% of the theoretical values assuming Gaussian pulse shapes (i.e., $g_p^{(2)} = 0.66$). Measured $g_p^{(2)}$ for the soliton pulse after the microscope was 0.53 (assuming a FWHM pulse duration of 76 fs). This reduces our expected signal improvement from 52 times to 41.8 times with the soliton source when the same excitation power is used at the sample.

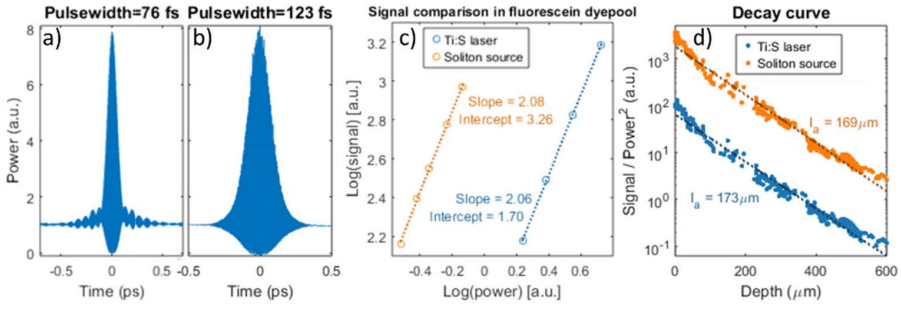

Fig. 4. Second order autocorrelation traces recorded after the microscope for the 940 nm pulse from (a) the soliton and (b) the Ti:S oscillator (GaAsP photodiode, deconvolution factor = 1.4) Signal from the soliton source and Ti:S laser (c) in a fluorescein dye-pool and (d) as a function of imaging depth for *in vivo* mouse brain imaging.

To minimize the effect of spatial mismatch in the beam profiles, we used telescopes to overfill the back aperture of the objective. Two-photon fluorescence signal from the two sources was measured in the thick sample limit, i.e., a 20 µM fluorescein dye pool. Bandpass

Biomedical Optics EXPRESS

filters were used before the PMT to ensure that no second-harmonic signal was collected. The soliton source produced 36.2 times more signal than the Ti:S laser for the same average power, and the results are shown in Fig. 4(c). The slight deviation from the theoretical value is likely due to differences in experimental conditions such as small differences in the beam spatial profiles, and the temporal pulse quality.

Finally, we compared the performance of the two sources in *in vivo* mouse brain imaging. A craniotomy was performed on an 8-week-old wild type mouse, and a glass window was inserted to observe the brain. Fluorescein-dextran was injected retro-orbitally and observed in the brain vasculature. Each stack of images was obtained with both sources. A few frames from each stack were measured at different power levels to ensure that there was no fluorescence saturation. Normalized images obtained using each source are shown in Fig. 5.

To quantify the signal from both sources, 332 regions with areas of 100-500 μm^2 were selected. The average signal for the soliton source was 26.3 ± 4.1 times higher than that of the Ti:S laser at the same average power, which shows that an average power reduction of 5.1 ± 0.4 times can be achieved using the soliton source. The attenuation lengths for both sources were ~170 μm which is similar to values reported in previous publications [3]. The difference in performance enhancement compared to that in the fluorescein dye-pool is possibly due to the differences in the beam spatial profiles from the two sources combined with scattering and wave-front aberrations in the mouse [23]. This is supported by the slight difference in the scattering lengths, which over a range of 4 scattering lengths is equivalent to approximately 20% change in the relative signal improvement for the surface layers versus the deepest layers.

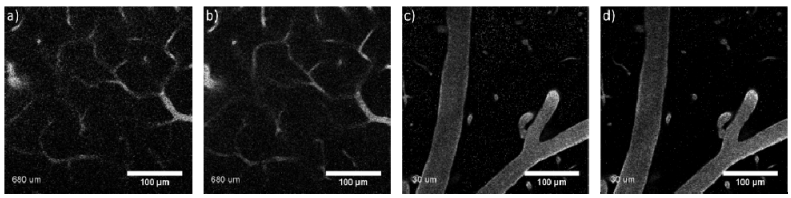

Fig. 5. Fluorescein-labeled mouse brain vasculature recorded with both sources. Images were recorded at comparable fluorescence levels, and have been further normalized to emphasize that there is no difference in image quality. (a),(c) Ti:S laser; (b),(d) Soliton source. Imaging depth from surface of the brain is 680 μm for (a) and (b) and 30 μm for (c) and (d).

6. Discussion

Tissue damage due to heating is clearly reduced by reducing the repetition rate and increasing the pulse peak intensity while keeping the average power constant. However, there is a possibility of increased nonlinear photodamage and photobleaching. Therefore, deep tissue multiphoton imaging is a trade-off between linear (i.e., thermal) damage and higher order nonlinear photodamage or photobleaching. The relationship between photobleaching and the pulse characteristics can be complicated. There have been a number of measurements in the past to elucidate the mechanisms of photodamage and photobleaching. Several papers have shown higher than 2nd order nonlinear damage/bleaching in 2-photon imaging [24–26], which suggest that higher repetition rates could be beneficial. However, a recent paper has shown insignificant difference in the photobleaching rate when changing the excitation repetition rate by more than 20 times [27]. There are several previous papers showing that shorter laser pulses reduce the rate of photobleaching when normalized to the same 2-photon fluorescence generation [28–30], which appear to be inconsistent with the mechanism of higher than 2nd order nonlinear photobleaching. Another paper demonstrated that photodamage of neurons is reduced by temporal gating at 2.4 MHz and 1.2 MHz of the 80-MHz pulse train, while further reduction of the gating frequency to 0.4 MHz appears to increase the photodamage [8]. When excited state or triplet state absorption is involved in the photobleaching pathway, lower repetition rate can significantly improve total fluorescence

Biomedical Optics EXPRESS

yield before molecular bleaching [31]. The discrepancies of previous findings on photodamage and photobleaching may be caused by the differences in the sample, the fluorophores, imaging conditions (e.g., *in vivo* or *in vitro*), excitation wavelength, assessment methods, etc. While this brief discussion is not meant to be exhaustive or definitive, photodamage and photobleaching are important considerations when optimizing the pulse repetition rate in addition to tissue heating and fluorophore saturation discussed in this paper. On the other hand, the pulse energy used in this paper (e.g., Fig. 5, ~0.15 nJ at the focus) is significantly below the nonlinear damage threshold for cultured cells [32, 33], and approximately 50 to 100 times below the nonlinear ablative damage threshold [34, 35]. Pulse energy much higher than the value used in this paper has been used in the past for *in vivo* 2-photon imaging of the mouse brain [3,6].

7. Conclusion

We analyzed the optimum repetition rate for increasing the efficiency of two-photon signal generation deep within scattering samples. Based on the properties of commonly used fluorophores, the ideal repetition rate for deep tissue two-photon imaging is significantly lower than 80 MHz, which is typically provided by mode-locked Ti:S oscillators, and significantly higher than 1 MHz, which is typically provided by OPAs pumped by amplifier systems. We present a fiber-based, wavelength tunable source that can provide tunable repetition rate between 1 and 10 MHz, and pulse energies between 26.4 nJ (830 nm) and 80 nJ (1000 nm). We compared the performance of our source to a Ti:S oscillator and found that we could obtain the same two-photon excited signal deep inside a mouse brain with approximately 5.1 times less average power, and with pulse energy still significantly below the limit for fluorescence saturation and nonlinear photodamage. Our results may motivate further development of a low-cost and robust excitation source that provides the optimum pulse characteristics for deep tissue two-photon microscopy in the wavelength range between 900 and 1000 nm.

Funding

NIH/NIBIB (R01EB017274); National Science Foundation NeuroNex Grant (DBI-1707312).

Acknowledgment

The authors thank Will Renninger, Logan Wright, Dimitre Ouzounov, David Sinefeld and Tianyu Wang for helpful discussions.

Disclosures

The authors declare that there are no conflicts of interest related to this article.

128.84.126.254 {ts '2019-08-02 11:28:50'}